5-2021

Assignment of Local Coordinate Systems and Methods to Calculate Tibiotalar and Subtalar Kinematics: A Systematic Review

Amy L. Lenz
University of Utah

Marisa A. Strobel
Marquette University

Abigail M. Anderson
Marquette University

Alissa Fial
Marquette University, alissa.fial@marquette.edu

Bruce A. MacWilliams
University of Utah

See next page for additional authors

Journal of Biomechanics, Vol. 120, (May 2021): 110344. DOI.

Assignment of Local Coordinate Systems and Methods to Calculate Tibiotalar and Subtalar Kinematics: A Systematic Review

Amy L. Lenz
Department of Orthopaedics, University of Utah, Salt Lake City, UT, United States
Marisa A. Strobel
Department of Biomedical Engineering, Marquette University, Milwaukee, WI, United States
Abigail M. Anderson
Department of Biomedical Engineering, Marquette University, Milwaukee, WI, United States
Alissa V. Fial
Research & Instruction Services, Marquette University, Milwaukee, WI, United States
Bruce A. MacWilliams
Department of Orthopaedics, University of Utah, Salt Lake City, UT, United States
Motion Analysis Center, Shriners Hospitals for Children-Salt Lake City, Salt Lake City, UT, United States
Joseph J.Drzak
Physical Therapy Program, Midwestern University, Downers Grove, IL, United States
Motion Analysis Center, Shriners Hospitals for Children-Chicago, Chicago, IL, United States

Karen M. Kruger
Department of Biomedical Engineering, Marquette University, Milwaukee, WI, United States
Motion Analysis Center, Shriners Hospitals for Children-Chicago, Chicago, IL, United States

Abstract

The introduction of biplane fluoroscopy has created the ability to evaluate *in vivo* motion, enabling six degree-of-freedom measurement of the tibiotalar and subtalar joints. Although the International Society of Biomechanics defines a standard method of assigning local coordinate systems for the ankle joint complex, standards for the tibiotalar and subtalar joints are lacking. The objective of this systematic review was to summarize and appraise the existing literature that (1) defined coordinate systems for the tibia, talus, and/or calcaneus or (2) assigned kinematic definitions for the tibiotalar and/or subtalar joints. A systematic literature search was developed with search results limited to English Language from 2006 through 2020. Articles were screened by two independent reviewers based on title and abstract. Methodological quality was evaluated using a modified assessment tool. Following screening, 52 articles were identified as having met inclusion criteria. Methodological assessment of these articles varied in quality from 61 to 97. Included articles adopted primary methods for defining coordinate systems that included: (1) anatomical coordinate system (ACS) based on individual bone landmarks and/or geometric shapes, (2) orthogonal principal axes, and (3) interactive closest point (ICP) registration. Common methods for calculating kinematics included: (1) joint coordinate system (JCS) to calculate rotation and translation, (2) Cardan/Euler sequences, and (3) inclination and deviation angles for helical angles. The methods each have strengths and weaknesses. This summarized knowledge should provide the basis for the foot and ankle biomechanics community to create an accepted standard for calculating and reporting tibiotalar and subtalar kinematics.

Keywords

Systematic review, Coordinate systems, Hindfoot kinematics, Subtalar, Tibiotalar, Anatomical axes

Abbreviations

ACS, Anatomical Coordinate System
AP, Anteroposterior or Anterior/Posterior
ICP, Iterative Closest Point
ISB, International Society of Biomechanics
JCS, Joint Coordinate System
ML, Medial/Lateral
SI, Superior/Inferior
WBCT, Weightbearing Computed Tomography

1. Introduction

Ankle kinematics are commonly evaluated using skin-based motion capture techniques. Traditionally, these experimental methods combine the contributions of the tibiotalar and subtalar joints and are reported as hindfoot kinematics due to the lack of reliable palpable talar landmarks for skin-based motion capture (MacWilliams et al., 2003). Furthermore, the tibia and fibula are considered to be a rigid body with an axis defined across the medial and lateral malleoli, anatomically describing the talocrural joint rather than isolating the tibiotalar axis (i.e. articulation solely between the tibia and talus). With any marker-based gait analysis, skin

motion artifact is always a concern. In the foot, it has been shown to cause errors ranging 2.7–14.9 mm (Maslen and Ackland, 1994).

In 2002, the International Society of Biomechanics (ISB) proposed a general reporting standard for joint kinematics for the ankle, hip, and knee (Wu et al., 2002). In this report, experts recommended the ankle joint was to be comprised of the combined talocrural and subtalar joints and those standards for assigning coordinate systems for tibiotalar and subtalar joint kinematics could be addressed at a later time. The ISB standard has begun to gain more wide-spread use, however a consensus method for defining separate anatomic coordinate systems for the tibiotalar and subtalar joints has still not been established.

With the advent of volumetric high-resolution medical imaging and biplane fluoroscopy techniques, it is possible to measure *in vivo* kinematics of the tibiotalar and subtalar joints separately. Biplane fluoroscopy is an emerging technology that provides a means to track the 3-D kinematics of these joints directly (Cross et al., 2017). It employs two x-ray images that are aligned with digitally reconstructed radiographs created from volumetric computed tomography (CT) scans, thus enabling visualization of specific bones during functional movements. With the introduction of weightbearing CT scans (WBCT), a detailed analysis of the hindfoot under a static weightbearing condition has also become possible (Barg et al., 2018). When evaluated individually using these imaging techniques, the tibiotalar and subtalar joints can be reported in unique six degree-of-freedom articular contributions to the ankle joint complex with sub-millimeter and degree precision (Wang et al., 2015a). Yet, to reliably and consistently report tibiotalar and subtalar kinematics, individual bone coordinate systems and associated mathematical definitions are needed for calculating joint rotations and translations.

Several authors have assigned coordinate systems to individual bones based on their individual anatomy or geometric principal axes (Campbell et al., 2016, Claassen et al., 2019, de Asla et al., 2006, Green et al., 2011). Other investigators assigned coordinate systems where the axes of the talus and calcaneus were parallel to the tibia axis (i.e. tibia-aligned) (Roach et al., 2016b, Wang et al., 2015a). As a result, there are many individualized hindfoot bone coordinate system definitions and it is sometimes unclear what effect these numerous strategies have on the resulting kinematics. Recent work presented a comparison of the kinematics from the tibia-aligned and bone-independent coordinate systems showed variability among subjects, joints, and plane of motion (Kruger et al., 2019b). Comparison between these coordinate systems showed mean offsets in kinematic curves of up to 45° and excursion differences of up to 6° in all three planes of motion.

Furthermore, kinematic mathematical methods are inconsistent across the biomechanics community and can include various methods including the joint coordinate system (JCS), Cardan/Euler rotation sequences, and helical axes definitions (Grood and Suntay, 1983, Ledoux et al., 2006, Woltring et al., 1994). While the JCS and Cardan/Euler rotation sequences are often treated as different methods of calculation of kinematics, it is not commonly appreciated that the JCS is equivalent to a specified Cardan sequence (MacWilliams and Davis, 2013). With infinite combinations of coordinate systems and kinematic definitions, the lack of a foot and ankle biomechanics community standard for reporting tibiotalar and subtalar joint motion can often make it difficult to compare results across multiple publications, laboratories, and institutions. Consensus is even lacking for defining the talocrural joint (articulation between the tibia, talus and calcaneus) versus the tibiotalar joint (articulation between the tibia and talus) (Fig. 1). The clinical implications for inconsistent reporting techniques can be detrimental if experimental data analysis is used as a pre-surgical evaluation tool or for assessing post-operative outcomes. These research and clinical concerns illustrate the need to establish a consensus for coordinate system construction and kinematic reporting as biplane fluoroscopy assessment becomes more wide-spread.

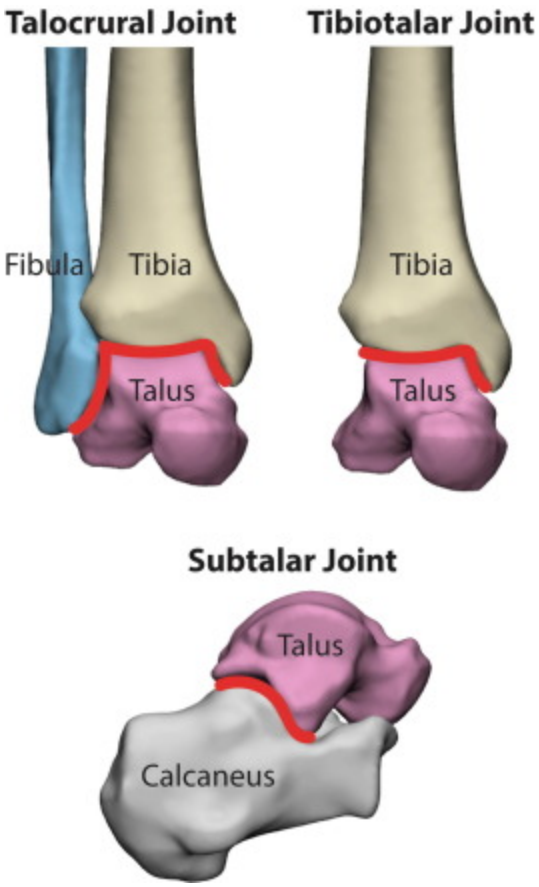

Fig. 1. Joint definitions for the talocrural, tibiotalar and subtalar articulations. The red line indicates the bone articulation interactions of interest which are contained in the respective joints. (For interpretation of the references to colour in this figure legend, the reader is referred to the web version of this article.)

With a growing wealth of foot and ankle biomechanics literature, there is a need to summarize current strategies for defining coordinate systems and calculating kinematics, as well as thoroughly evaluate the strengths and weaknesses of current methods. Therefore, the objective of this review was to summarize and appraise existing literature that either (1) defined coordinate systems for the tibia, talus, and/or calcaneus or (2) assigned kinematic mathematical definitions for the tibiotalar or subtalar joints. This knowledge should provide the basis for foot and ankle biomechanics community discussions to create an accepted standard for reporting tibiotalar and subtalar kinematics.

2. Methods

2.1. Search strategy

A systematic literature search was developed with the assistance of a health sciences librarian. The following databases were searched: PubMed, Engineering Village and Web of Science. The search results were limited to English Language, and the date range selected was 2006 through April 2020. The initial search was developed in PubMed using a combination of database controlled vocabulary, Medical Subject Terms (MeSH) and keywords. The search was refined based upon pre-selected articles relevant to the topic and the search question. Once the initial search was developed in PubMed, keywords were utilized to fit the parameters of the other two databases.

The parameters included a focus on the foot, ankle, joints, range of motion as well as techniques and equipment for measurement. In addition, there was a concentration on excluding terminology related to the knee and femur. Sample terms used in the search included “foot”, “bones of the feet”, “calcaneus”, “tibiotalar joint”, “subtalar joint”, “*in vivo* kinematics”, “3-D imaging”, “fluoroscopy”, and “biplane radiography.” The complete strategies can be found in Appendix A.

After removing duplicates, remaining articles were screened by two independent reviewers based on the title and abstract. The articles were classified as “yes” or “no” based on the criteria in Table 1. Inclusion criteria was defined to limit included studies to those that would be done in larger study populations of *in vivo* bone motion tracking and thus, excluded invasive methods such as implanted tantalum beads. Disagreements between the two raters were resolved through discussion with other co-authors.

Table 1. Article selection inclusion and exclusion criteria.

Inclusion Criteria	**Exclusion Criteria**
• Use 3D imaging (CT or MRI) • Mention of ankle joint complex • Defined coordinate system used **or** calculated 3D kinematics	• Only plain film radiographs and/or slice evaluations of CT and/or EOS • Assumed single functional joint model in ankle joint complex • Animal model • Only muscle movement analyzed • Invasive evaluation methods

2.2. Data extraction

The following descriptive characteristics of included studies were extracted and summarized: authors, participant ages, presence of pathology, sample size, activity performed during data collection, type of fluoroscopic imagining technique (e.g. single or biplane), 3D geometry source, coordinate system definition, and kinematic modeling method. To summarize the strategies used to define coordinate systems, included studies were initially reviewed and classified as either using an anatomic coordinate system, ICP, or principal axes. Studies that used an anatomic coordinate system were further categorized as either using landmarks, geometric shape fitting, or a combination of both techniques. For studies using anatomic landmarks, individual segment locations used to attach the Cartesian coordinate system were identified and summarized. For studies using geometric shape fitting, the geometric primitive type (e.g. sphere, cylinder, etc.) and the anatomic surface/point(s) on the surface were identified and summarized. To summarize the strategies used assign kinematic mathematical definitions for the tibiotalar or subtalar joints, included studies were categorized as either using JCS, Cardan/Euler Angles, or Helical Axis. Additionally, de-rotation sequences and the assignment of primary and secondary axes were identified and summarized.

2.3. Methodological quality assessment of included literature

The methodological quality of the included studies was evaluated using a modified assessment tool based on the QUACS (Quality Appraisal for Cadaveric Studies) scale and a metric introduced by Trinler et al. (Table 2) (Trinler et al., 2018, Wilke et al., 2015). The combination of these two scales allowed for components of the QUACS scale which were appropriate to assess coordinate system definitions and components of the Trinler metric which were most appropriate for assessing kinematic calculations to be combined into one metric. Two reviewers independently examined each included study using the evaluation checklist and reported scores as a percentage (total points assigned out of possible 44 points). Agreement between raters for the summed methodological

score was assessed using a two-way random intraclass correlation coefficient (ICC). Agreement was considered to be very good for an ICC > 0.80; good with an ICC = 0.61 to 0.80; moderate with an ICC = 0.41 to 0.60; fair with an ICC = 0.21 to 0.4; and poor with an ICC < 0.20 (Yeung et al., 2015). These scores were then pooled and reported as an average.

Table 2. Modified Trinler et al and QUACS Assessment Criteria.

Categories	**Purpose**		**Scale**
Statement of Aims	Aims clearly stated, hypothesis is presented		1–3
Description of Participants	Basic Information About Sample is Included (Age, gender, sample size & foot pathologies)		1–3
Methods	Clearly structured, detailed outline of the study protocol. Mentions coordinate system used and/or kinematic calculations		1–5
Description of Measurement Equipment	States what system was used to capture images with details (i.g. CT/MRI slice thickness)		1–3
Consistency of findings	Made some form of reliability or validation check for their data, whether it be for kinematic or coordinate system calculations or for the imaging set up (CT, MRI or fluoroscopy)		1–5
Description of Kinematic Modeling	Description of coordinate system and/or modeling technique		1–5
Description of Measurement Output	Results presented thoroughly and precise	Description of measurement output and corresponding statistical methods (Results described thoroughly with units and spread, appropriate statistical methods applied)	1–5
	Statistical Methods	Correct choice and application of statistical data analysis	1–3
	Figures of data are included	Figures of key data (e.g coordinate systems) with precise labels are included	1–3
Statement of Discussion and Conclusion	Study is discussed within the context of current evidence	Other relevant trials relating to the field of study are stated and discussed	1–3
	Clinical implications of the results are discussed	Similar studies are reported, added knowledge and its relevance to the field are pointed out	1–3

Categories	Purpose		Scale
	Limitations of the study are addressed	Weakness and methodological shortcomings are reported (note mentioned ankle pathologies)	1–3

3. Results

The search strategies had a total yield of 922. After removing duplicates, the total number of articles was reduced to 757. The initial screening between the two reviewers for screening and manuscripts requiring full evaluation was 95%. Following the screening, 52 articles were identified as having met inclusion criteria and utilized a 3D imaging modality, made mention of the ankle joint complex, and either defined a coordinate system or calculated *in vivo* or *ex vivo* 3D kinematics (Table 3). A flowchart of the systematic search process is visualized in Fig. 2.

Table 3. Summary of included articles.

Article	Age range	Known ankle pathologies	# of subjects	Activity during collection	3D Geometry Source	Coordinate system	Kinematic modeling	Dynamic Fluoroscopy Imaging
(Beimers et al., 2008)	22–35 years	No known pathology	20	Supine, leg fixed	CT	Principal axes	Helical axes	n/a
(Cao et al., 2019a)	19–39 years	Unilateral CAI	11	Walking	WBCT	Landmark ACS and ICP	Cardan/Euler	biplane
(Cao et al., 2019b)	19–30 years	Healthy, unilateral LAS copers, and unilateral FAI	30	Walking	WBCT	Landmark ACS	Cardan/Euler	biplane
(Caputo et al., 2009)	19–57 years	Unilateral ankle sprain, unilateral ATFL, or CFL	9	Step down	MRI	ICP and geometric ACS	JCS	biplane
(Cho et al., 2014)	48–94 years	No known pathology	61	Not reported	CT	Landmark ACS and principal axes	Helical axes	n/a
(Claassen et al., 2019)	44–104 years	No known pathology	98	Not reported	CT	Landmark ACS	Not reported	n/a
(Clarke et al., 2015)	22–48 years	No known pathology	10	Prone	MRI	ICP	Helical axes	n/a
(de Asla et al., 2006)	32–43 years	No known pathology	5	Supine during MRI, non and	MRI	Geometric ACS	Cardan/Euler	biplane

Article	Age range	Known ankle pathologies	# of subjects	Activity during collection	3D Geometry Source	Coordinate system	Kinematic modeling	Dynamic Fluoroscopy Imaging
				WB fluoroscopy				
(Fassbind et al., 2011)	44 – 60 years	No known pathology	10	Non-WB	MRI	Principal axes	Helical axes and Cardan/Euler	n/a
(Fukano and Fukubayashi, 2014)	22 – 25 years	No known pathology	7	Downward step	CT	Landmark and geometric ACS	JCS	single
(Fukano et al., 2018)	21– 27 years	No known pathology	17	Walking	CT	Landmark and geometric ACS	JCS	single
(Fukano et al., 2020)	20– 25 years	History of ankle sprain and healthy	18	Walking	CT	Landmark and geometric	JCS	single
(Goto et al., 2009)	Mean 23.8 years	No known pathology	4	Non-weightbearing, passive fixation	MRI	Landmark ACS	Cardan/Euler and Helical axes	n/a
(Green et al., 2011)	25– 28 years	No known pathology	10	Simulated Weightbearing CT	CT	Landmark and geometric ACS	Not reported	n/a
(Hayes et al., 2006)	30– 50 years	Unilateral ankle osteoarthritis	21	Not reported	CT	Landmark ACS	Not reported	n/a
(Imai et al., 2009)	21– 35 years	No known pathology	10	Not reported	CT	Principal axes	Cardan/Euler	n/a
(Imai et al., 2011)	2– 86 years	Normal, stage II PTTD, stage III PTTD	10	Supine, non-WB	CT	ICP	Cardan/Euler	n/a
(Ito et al., 2015)	78 years	No known pathology	1	Robotic gait simulator	CT	Landmark ACS	Cardan/Euler	biplane
(Iwamoto et al., 2014)	49– 71 years	RA patients underwent TAA	10	Walking	CAD	Geometric ACS	Cardan/Euler	single

Article	Age range	Known ankle pathologies	# of subjects	Activity during collection	3D Geometry Source	Coordinate system	Kinematic modeling	Dynamic Fluoroscopy Imaging
(Kleipool et al., 2016)	19–59 years	Ankle inversion instability	12	Flexion	CT	Principal axes	Helical axes	n/a
(Kleipool et al., 2019)	23–59 years	No known pathology	20	Supine, simulated Weightbearing CT	CT	Geometric ACS	Helical axes	n/a
(Kobayashi et al., 2013)	20–46 years	Unilateral FAI	5	Food fixated	WBCT	Landmark and geometric ACS	Cardan/Euler	single
(Kobayashi et al., 2014a)	19 – 24 years	Unilateral CAI	14	Not reported	CT	Landmark and geometric ACS; ICP	Cardan/Euler	single
(Kobayashi et al., 2014b)	19–24 years	Unilateral CAI	14	Passive ankle rotation	WBCT	Landmark and geometric ACS; ICP	Cardan/Euler	single
(Kobayashi et al., 2015)	18–26 years	Unilateral FAI	12	Passive ankle rotation	WBCT	Landmark and geometric ACS; ICP	Cardan/Euler	single
(Koo et al., 2015)	19–24 years	No known pathology	10	Walking	CT	Geometric ACS	JCS	biplane
(Kozanek et al., 2009)	44–69 years	Post-traumatic tibiotalar osteoarthritis	6	Walking, non-WB MRI	MRI	Geometric ACS	Cardan/Euler	biplane
(Ledoux et al., 2006)	18–75 years	Pes cavus, no known, and pes planus	40	Simulated Weightbearing CT	CT	Principal axes	Cardan/Euler	n/a
(Lenz et al., 2020)	Not reported	Tibiotalar arthrodesis	10	Walking	WBCT	Landmark and geometric ACS	JCS	biplane
(Leszko et al., 2008)	44–83 years	Salto TAA	20	Walking and stair ascension	CAD	Landmark ACS	JCS	single
(Liu et al., 2007)	39–71 years	RA hindfoot valgus	22	Neutral and Non-WB	CT (RA) and MRI	Landmark ACS	Cardan/Euler	n/a

Article	Age range	Known ankle pathologies	# of subjects	Activity during collection	3D Geometry Source	Coordinate system	Kinematic modeling	Dynamic Fluoroscopy Imaging
		deformity and no known pathology			(no known)			
(Maharaj et al., 2020)	Not reported	No known pathology	6	Prone, non-WB	CT	Landmark ACS	Cardan/Euler	biplane
(Makki et al., 2019)	Mean 12 years	No known pathology	6	Dynamic, orthotic fixture used	MRI	Landmark ACS	Cardan/Euler	n/a
(Mattingly et al., 2006)	18–30 years	No known pathology	6	Supine and non-WB	MRI	Principal axes	Cardan/Euler	n/a
(Nichols et al., 2016)	24–38 years	No known pathology	10	Walking	CT	Landmark and geometric ACS	Cardan/Euler	biplane
(Nichols et al., 2017)	24–38 years	No known pathology	10	Walking	CT	Geometric ACS	Cardan/Euler	biplane
(Nozaki et al., 2016)	20–49 years	No known pathology	50	Not reported	CT	Landmark and geometric ACS	Not reported	n/a
(Nozaki et al., 2017)	20–49 years	No known pathology	50	Not reported	CT	Landmark ACS	Not reported	n/a
(Nozaki et al., 2019)	23–84 years	No known pathology	44	Not reported	CT	Landmark and geometric ACS	Not reported	n/a
(Parr et al., 2012)	Not reported	No known pathology	58	Not reported	CT and MRI	ICP and geometric ACS	Helical axes	n/a
(Roach et al., 2016a, Roach et al., 2016a)	24–38 years	No known pathology	10	Heel rise & walking	CT	Landmark and geometric ACS	JCS	biplane
(Roach et al., 2017)	24–38 years	No known & CAI	14	Heel rise & walking	CT	Landmark and geometric ACS	JCS	biplane

Article	Age range	Known ankle pathologies	# of subjects	Activity during collection	3D Geometry Source	Coordinate system	Kinematic modeling	Dynamic Fluoroscopy Imaging
(Van Sint Jan et al., 2006)	50 years old	No known pathology	1	Non-WB	CT	Landmark ACS	JCS	n/a
(Wainright et al., 2012)	33–41 years	Corrected unilateral mechanical LAI	7	Standing	MRI	ICP and geometric ACS	JCS	biplane
(Wan et al., 2006)	24–45 years	No known pathology	7	Walking	MRI	Not reported	Cardan/Euler	biplane
(Wang et al., 2015a, Wang et al., 2015b)	52–81	No known pathology	2	Not reported	CT	Landmark and geometric ACS	JCS	biplane
(Chen Wang et al., 2016)	36–52 years	No known pathology	7	Walking	CT	Geometric ACS	JCS	single
(Wolf et al., 2007)	28–35 years	No known pathology	3	Simulated WB	MRI	ICP	Helical axes	n/a
(Wolf et al., 2008)	28–35 years	No known pathology	8	Simulated WB	MRI	ICP	Helical axes	n/a
(Xu et al., 2015)	21–44 years	No known & stage II PTTD	40	Supine	CT	Not reported	Cardan/Euler	n/a
(Yamaguchi et al., 2009)	23–42 years	No known pathology	7	WB and non-WB fluoroscopy	CT	Landmark and geometric ACS	JCS	single
(Zhang et al., 2019)	18–40 years	No known & FAI	18	Walking	CT	Geometric ACS	JCS	biplane

ATFL = Anterior Talofibular Ligament, CAI = Chronic Ankle Instability, CFL = Calcaneofibular Ligament, FAI = Functional Ankle Instability, LAS = Lateral Ankle Sprain, LAI = Lateral Ankle Instability, PTTD = Posterior Tibial Tendon Dysfunction, RA = Rheumatoid Arthritis, TAA = Total Ankle Arthroplasty, WB = Weight Bearing, CT = Conventional Computed Tomography, WBCT = Weight Bearing Computed Tomography, MRI = Magnetic Resonance Imaging.

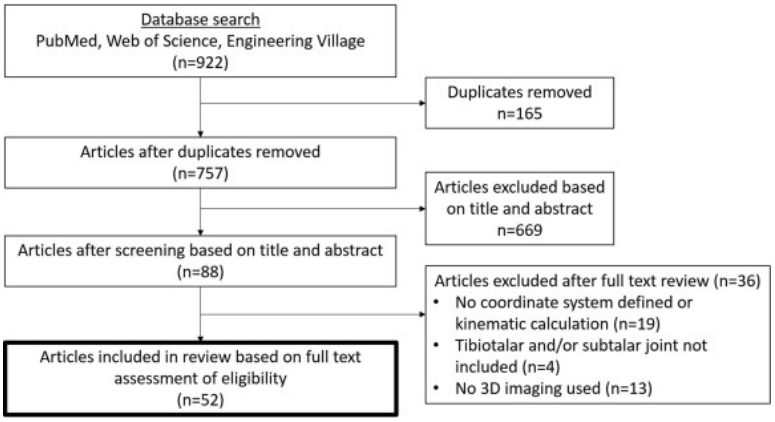

Fig. 2. Flowchart of article selection process.

3.1. Methodologic quality assessment of included articles

The average methodologic score was 87. The lowest scoring columns were clinical implications of results (79), description of kinematic modeling (79), and consistency of findings (71) (Table 4). The article with the lowest methodologic quality assessment score was 61 (Parr et al., 2012). The highest scoring articles were scored 97 (Fukano et al., 2018, Fukano et al., 2020, Lenz et al., 2020, Roach et al., 2016b). In total, seven articles scored above 95 (Caputo et al., 2009, Wan et al., 2006, Yamaguchi et al., 2009) and 3 articles scored below 75 (Green et al., 2011, Hayes et al., 2006, Parr et al., 2012). Agreement between raters for the total summed methodological score was 0.99, which is considered very good.

Table 4. Individual scores for each category of methodologic bias assessments. Scores are reported as percentage (%) and total is average of all categories for each study.

Article	Statement of Aims	Description of Participants	Methods	Description of Measurement Equipment	Consistency of Findings	Description of Kinematic Modeling	Results Presented Thoroughly and Precise	Statistical Methods	Figures of Data are Included	Study is Discussed within the Context of Current Evidence	Clinical Implications of Results Discussed	Limitations Addressed	Totals
(Beimers et al., 2008)	67	100	80	100	60	80	100	67	100	100	100	67	85
(Cao et al., 2019a)	100	100	100	67	60	80	100	100	67	100	100	100	89
(Cao et al., 2019b)	100	100	80	67	60	80	100	100	100	100	100	100	91
(Caputo et al., 2009)	100	100	100	67	100	80	100	100	100	100	100	100	96
(Cho et al., 2014)	67	100	80	100	40	80	100	100	100	100	67	33	81
(Claassen et al., 2019)	67	100	100	100	100	80	60	100	100	100	67	100	89
(Clarke et al., 2015)	67	100	80	100	100	80	80	67	100	100	67	100	87
(de Asla et al., 2006)	67	100	80	100	40	100	100	100	100	100	100	67	88
(Fassbind et al., 2011)	67	100	80	100	60	60	80	67	100	67	67	100	79
(Fukano and Fukubayashi, 2014)	100	67	80	67	100	100	80	100	100	100	100	100	91
(Fukano et al., 2018)	67	100	100	100	100	100	100	100	100	100	100	100	97

(Fukano et al., 2020)	100	100	100	100	100	100	100	100	100	67	100	100	97
(Goto et al., 2009)	67	100	80	100	40	80	100	33	100	100	67	100	81
(Green et al., 2011)	67	100	80	33	20	40	100	100	100	67	100	67	73
(Hayes et al., 2006)	67	100	60	100	20	80	80	100	100	33	33	67	70
(Imai et al., 2009)	100	100	80	67	40	60	100	100	100	33	67	100	79
(Imai et al., 2011)	67	100	80	100	60	60	100	100	100	100	33	100	83
(Ito et al., 2015)	67	100	80	67	80	80	100	67	100	100	67	100	84
(Iwamoto et al., 2014)	100	100	100	67	60	100	80	100	100	100	100	100	92
(Kleipool et al., 2016)	100	100	60	100	60	60	60	100	100	100	67	100	84
(Kleipool et al., 2019)	100	67	80	67	40	80	100	100	100	100	67	100	83
(Kobayashi et al., 2013)	100	100	100	67	80	100	80	100	100	100	100	100	94
(Kobayashi et al., 2014a)	100	100	100	67	40	80	60	100	100	100	67	100	84
(Kobayashi et al., 2014b)	100	100	80	67	60	80	80	100	100	100	100	100	89
(Kobayashi et al., 2015)	100	100	80	67	60	60	100	100	100	100	100	100	89
(Koo et al., 2015)	67	100	100	67	40	100	100	67	100	100	67	100	84
(Kozanek et al., 2009)	100	67	80	100	80	80	60	67	100	100	67	100	83
(Ledoux et al., 2006)	100	67	100	100	100	80	100	100	100	100	33	100	90

(Lenz et al., 2020)	100	100	100	100	80	80	100	100	100	100	100	100	97
(Leszko et al., 2008)	67	100	80	33	80	80	100	67	100	100	100	67	81
(Liu et al., 2007)	67	100	80	100	100	80	100	100	100	100	67	100	91
(Maharaj et al., 2020)	100	67	80	67	100	80	100	100	100	100	67	100	88
(Makki et al., 2019)	67	67	80	67	100	80	80	100	100	100	100	33	81
(Mattingly et al., 2006)	67	100	80	100	100	80	100	100	100	100	67	67	88
(Nichols et al., 2016)	100	100	80	67	80	80	100	100	100	67	67	67	84
(Nichols et al., 2017)	100	100	100	100	80	80	100	100	100	100	67	100	94
(Nozaki et al., 2016)	100	100	80	100	80	80	100	100	100	67	100	67	89
(Nozaki et al., 2017)	100	100	80	100	80	80	100	100	100	100	100	100	95
(Nozaki et al., 2019)	67	100	80	100	80	100	100	100	100	67	100	100	91
(Parr et al., 2012)	67	33	60	67	20	80	100	100	100	33	33	33	61
(Roach et al., 2016a, Roach et al., 2016a)	67	100	100	100	80	80	40	100	100	100	100	100	89
(Roach et al., 2017)	100	100	100	100	100	100	100	100	67	100	100	100	97
(Van Sint Jan et al., 2006)	67	100	80	67	80	60	80	33	100	100	33	100	75
(Wainright et al., 2012)	100	100	80	67	60	80	80	100	67	100	100	100	86

(Wan et al., 2006)	67	100	100	100	100	80	100	100	100	100	100	100	96
(Wang et al., 2015a, Wang et al., 2015b)	67	100	100	100	100	60	100	100	67	100	67	100	88
(Chen Wang et al., 2016)	67	100	80	100	100	40	100	100	67	100	33	100	82
(Wolf et al., 2007)	100	100	80	100	60	60	80	67	100	100	33	100	82
(Wolf et al., 2008)	67	100	80	100	40	60	80	100	100	100	67	33	77
(Xu et al., 2015)	100	100	100	100	60	100	80	100	100	100	100	100	95
(Yamaguchi et al., 2009)	100	100	100	67	100	80	100	100	100	100	100	100	96
(Zhang et al., 2019)	100	100	80	100	40	80	100	100	100	100	100	67	89

3.2. Coordinate system definitions

All but two of the 52 articles defined a CS (Wan et al., 2006, Xu et al., 2015). The remaining 50 articles were classified as using a geometric or landmark-based anatomical coordinate system (ACS), principal axes, an iterative closest point (ICP) registration, or a combination of these methods.

3.2.1. Anatomical coordinate systems (ACS)

A full description of anatomic features and landmarks used to define coordinate systems is included in Table 5. Commonly used landmarks and geometric features are visualized in Fig. 3. Twelve articles defined a completely landmark-based ACS (Cao et al., 2019a, Cho et al., 2014, Claassen et al., 2019, Goto et al., 2009, Hayes et al., 2006, Ito et al., 2015, Leszko et al., 2008, Maharaj et al., 2020, Makki et al., 2019, Van Sint Jan et al., 2006). The landmark definition method recommended by the ISB (Wu et al., 2002) defined landmarks on the tibio-fibular complex that were widely implemented (Cho et al., 2014, Claassen et al., 2019, Goto et al., 2009, Leszko et al., 2008). Three articles used self-defined methods to describe their coordinate system (Hayes et al., 2006, Maharaj et al., 2020, Van Sint Jan et al., 2006). One author (Yamaguchi et al., 2009) defined separate origins for the tibia, talus, and calcaneus by using the medial and lateral edges of each bone to define axes used by other authors (Cao et al., 2019a,b). Liu et al. modified a previously defined ACS (Cappozzo et al., 1995) to define the medial and lateral malleoli on the tibia. Ito et al. used a previously described method (Gutekunst et al., 2013) which used four talus and four calcaneus landmarks to define subtalar articulation (Ito et al., 2015).

Table 5. Summary of local coordinate systems reported across the literature and categorized by types of coordinate system: landmark, geometric, or combination of landmark and geometric.

Landmark					
Articles	**Citation Used for Definition**	**Tibia**	**Talus**	**Calcaneus**	**Articles Citing This Definition**
(Cao et al., 2019a)	(Yamaguchi et al., 2009)	Line connecting ML and AP center points of distal tibia shaft as SI axis, origin at intersection with tibial plafond	Midpoint of PM and PL edge of trochlea tali	Most lateral point of posterior articular surface and most medial point of middle articular surface intersection as origin, lateral wall of calcaneus passing through origin	(Cao et al., 2019b)
(Cho et al., 2014)	(Wu et al., 2002)	MM, LM*, MC, LC, TT, IM, and IC	n/a	n/a	(Claassen et al., 2019, Goto et al., 2009, Leszko et al., 2008, Makki et al., 2019)
(Hayes et al., 2006)	Self-defined	MC and LC	Talar dome	n/a	n/a
(Ito et al., 2015)	(Gutekunst et al., 2013)	n/a	Posterior talus, anterior talus, medial talus, and lateral talus	Posterior calcaneus, anterior calcaneus,	n/a

				inferior calcaneus, and superior calcaneus	
(Liu et al., 2007)	(Cappozzo et al., 1995)	LM* and MM	Talar dome to determine centroid	Ridge of sustentaculum tali to determine centroid	n/a
(Maharaj et al., 2020)	Self-defined	MM, most lateral and superior aspects of tibia	n/a	n/a	n/a
(Van Sint Jan et al., 2006)	Self-defined	Most lateral aspect of lateral TC, most medial aspect of medial TC, lateral and medial tibial tuberosity, Gerdy's tubercle, LM*, and MM	n/a	Center of calcaneus tuberosity, sustentaculum tali, fibular trochlea	n/a
Geometric					
Articles	Original Definition	Tibia	Talus	Calcaneus	Other Articles Cited By
(Caputo et al., 2009)	Self-defined	Cylinder fit to shaft of tibia	Circle fit to talar dome	n/a	(Wainright et al., 2012)
(de Asla et al., 2006)	Self-defined	n/a	Series of circular arcs fit to talar trochlea	n/a	(Koo et al., 2015, Kozanek et al., 2009, Zhang et al., 2019)
(Iwamoto et al., 2014)	Self-defined	ML midline of inferior surface and AP midline	Circle fit to surface of talar implant in ML center	n/a	n/a
(Kleipool et al., 2019)	(Krähenbühl et al., 2016)	n/a	n/a	Cylinder of posterior facet, centroid in calcaneus from mean of vertices	n/a
(Parr et al., 2012)	(Beimers et al., 2008, Besl and McKay, 1992)	n/a	Sphere(s) fit to talar trochlea	Sphere(s) fit to calcaneal facets and sustentaculum tali	(Nichols et al., 2017)
(Chen Wang et al., 2016)	(Okita et al., 2014)	Sphere attached to tibia	Geometric centroid of talus	n/a	n/a
Landmark and Geometric					

Articles	Original Definition	Tibia	Talus	Calcaneus	Other Articles Cited By
(Fukano and Fukubayashi, 2014)	(Yamaguchi et al., 2009) and self-defined	Centroid of tibial plafond, AM and AL edges of tibial plafond	Circle circumscribing talar trochlea including the midpoint of AM and AL edges, PM and PL edges of trochlea	Line from most lateral point of posterior articular surface to most medial point of middle articular surface to define calcaneal origin	(Fukano et al., 2018, Fukano et al., 2020)
(Green et al., 2011)	(Wu et al., 2002) and self-defined	Intermalleolar line*, cylinder fit to fibula*	n/a	n/a	n/a
(Kobayashi et al., 2013)	(Yamaguchi et al., 2009) and self-defined	Geometric center points used to define SI axis for origin definition of tibial plafond, AM and AL edges	Circle fit to midpoints of AM, AL, PM, and PL; anterior and posterior edge of trochlea on circle	Most lateral and posterior points of articular surface connected to most medial point of middle articular surface to define origin,	(Kobayashi et al., 2014a, Kobayashi et al., 2015)
(Wang et al., 2015a, Wang et al., 2015b)	Self-defined	Cylinder fit to tibia to define SI axis, origin at SI and tibial plafond	Surface of talar trochlea fit to cylinder, origin at midpoint	Line from furthest lateral surfaces on posterior articulating ML and AP surface to medial edge of middle articulating surface, origin at midpoint	(Lenz et al., 2020, Nichols et al., 2016, Roach et al., 2017, Roach et al., 2016a, Roach et al., 2016a)
(Yamaguchi et al., 2009)	Self-defined	Line connecting ML and AP center points of distal tibia shaft as SI axis, origin at intersection with tibial plafond	Midpoint of PM and PL edge of trochlea tali, circle drawn to contain points, arc fit to circle, origin defined at center	Most lateral point of posterior articular surface and most medial point of middle articular surface intersection as origin, lateral wall of calcaneus passing through origin	(Nozaki et al., 2016, 2017)

*=Fibula Feature, AL = Anterolateral, AM = Anteromedial, AP = Anteroposterior, IC = Inter-Condylar, IM = Inter-Malleolar, LC = Lateral Condyle, LM = Lateral Malleolus, MC = Medial Condyle, ML = Mediolateral, MM = Medial Malleolus, PL = Posterolateral, PM = Posteromedial, TC = Tibial Condyle, TT = Tibial Tuberosity, SI = Superoinferior.

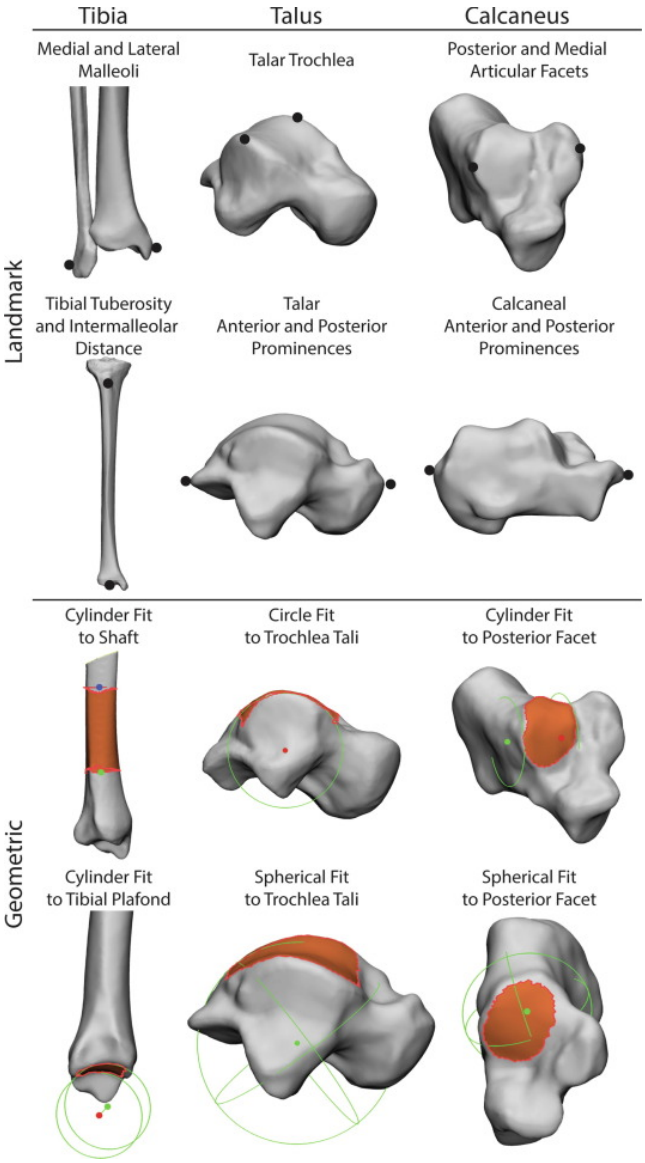

Fig. 3. Summary of most common landmark and geometric coordinate system axes definitions for the tibia, talus, and calcaneus. Black circles indicate the typical location for landmark selection. Orange selected surface regions are the surfaces used for an assignment of an axes using a geometric fit (cylinder, circle or sphere). Shown in green are the geometric fit objects with the axis or centroids visualized by red, green or red circles. (For interpretation of the references to colour in this figure legend, the reader is referred to the web version of this article.)

Eleven articles defined completely geometric-based ACS definitions (Caputo et al., 2009, Chen Wang et al., 2016, de Asla et al., 2006, Iwamoto et al., 2014, Koo et al., 2015, Kozanek et al., 2009, Nichols et al., 2017, Wainright et al., 2012, Zhang et al., 2019). The de Asla et al. geometric coordinate system was the most commonly cited (de Asla et al., 2006, Kozanek et al., 2009, Zhang et al., 2019); it used the talar trochlea fit into a series of circular arcs perpendicular to the transverse plane and the center of the sagittal plane arc to define the origin of the coordinate system. The coordinate system developed by Caputo et al. was used in a later paper (Wainright et al., 2012), that defined the neutral position with the ICP technique, a cylinder fit to the tibia shaft to define the proximal–distal axis, and a circle fit to the curve of the talar dome to define the origin in the sagittal plane. Nichols et al. created a geometric ACS using spheres and bone geometry to define tibiotalar and subtalar axes from the talus referencing previous work (Parr et al., 2012). Three other articles used less

commonly cited methods to develop a geometric coordinate system which is reported in Table 5 (Chen Wang et al., 2016, Iwamoto et al., 2014, Kleipool et al., 2019).

Sixteen articles defined a coordinate system using a combination of geometric and landmark-based features (Fukano and Fukubayashi, 2014, Fukano et al., 2018, Fukano et al., 2020, Green et al., 2011, Kobayashi et al., 2014a, Kobayashi et al., 2015, Lenz et al., 2020, Nichols et al., 2016, Nozaki et al., 2016, Nozaki et al., 2019, Roach et al., 2017, Roach et al., 2016b, Yamaguchi et al., 2009). Of these, nine used the components of the method described by Yamaguchi et al. (Fukano and Fukubayashi, 2014, Fukano et al., 2018, Fukano et al., 2020, Kobayashi et al., 2014a, Kobayashi et al., 2015, Nozaki et al., 2016). This method defined anteroposterior (AP), medial/lateral (ML), and superior/inferior (SI) axes with landmarks and used a combination of circles and arcs fit to the trochlea to define the origin of the talus. Wang et al. defined the tibia and calcaneus origins using a series of cylinder fits and the calcaneus using landmarks on the articular surface. This method was used by four other studies in this review (Chen Wang et al., 2016, Lenz et al., 2020, Nichols et al., 2016, Roach et al., 2017, Roach et al., 2016b). A modified version of the ISB recommended approach was also used where the ML axis was the intermalleolar midline from the medial malleolus to the lateral malleolus with the center defined as the origin, but a calculation of the axis was done from a cylindrical fit of the fibula (Green et al., 2011).

Of articles using anatomical coordinate systems, only three performed any form of repeatability analysis. Lui et al. analyzed CT scans of a cadaveric foot from three slice directions. They reported mean rotation error of 0.678 ± 0.238 and the mean translation error of 0.03 ± 0.01 mm (Liu et al., 2007). Fukano and Fukubayashi reported intra-rater repeatability of kinematic output with average differences from the mean of 0.60 mm for in-plane translations, 1.8 mm for out-of-plane rotations, and 0.59° for rotations (Fukano and Fukubayashi, 2014). Yamaguchi et al. performed the most comprehensive reliability assessment by assessing both inter- and intra-rater reliability for their coordinate system definition. They reported average inter-rater differences of 0.35 mm and 0.76° for translation and rotation, respectively. Reported average intra-rater differences were 0.35 mm and 0.85°, respectively (Yamaguchi et al., 2009).

3.2.2. Principal axes

Six articles exclusively used principal axes (Beimers et al., 2008, Fassbind et al., 2011, Imai et al., 2009, Ledoux et al., 2006, Mattingly et al., 2006). One article used principal axes combined with other methodologies (Kleipool et al., 2019). In a standard cartesian coordinate system, principal axes are three mutually perpendicular axes. Two articles (Beimers et al., 2008, Kleipool et al., 2019) defined the first principal axis of the talus as the AP axis, the second principal axis as the ML axis, and third principal axis as the SI axis. Fassbind et al. used a previously defined method (Schmidt, 1985) to define the principal axes which used bones at the neutral position and corresponding transformation matrices to determine positions. Imai et al. used a combination of principal axes and point clouds. Ledoux et al. provided a local coordinate system for each bone where the AP axis was the principal axes with the least inertia and the ML axis had the most inertia. Mattingly et al. employed a vector analysis method which was used to quantify translational motion between centroids at measured distances to determine principal axes of rotation from intersections at the geometric centroid of each bone.

3.2.3. Iterative closest point (ICP) registration

ICP and point cloud/set methods can be used to create a coordinate system that is not dependent on anatomical landmarks or geometric shape fitting to those landmarks. Four articles exclusively used iterative closest point (ICP) registration (Clarke et al., 2015, Imai et al., 2011, Wolf et al., 2007, Wolf et al., 2008). Of these articles, three used an ICP definition which was to determine the closest point pairs by registering data shapes to model shape primitives (Besl and McKay, 1992) (Clarke et al., 2015, Wolf et al., 2007, Wolf et al., 2008). Imai et al. utilized a previously defined method (Ochia et al., 2006) where a point cloud dataset was created for use in the volume merge method. The volume merge method involves a moving body in a neutral position being rotated

and translated toward the same body in a stationary and rotated position. Eight additional articles utilized the ICP technique with other methods (Cao et al., 2019a, Caputo et al., 2009, Imai et al., 2009, Kleipool et al., 2019, Kobayashi et al., 2014a, Kobayashi et al., 2015, Parr et al., 2012, Wainright et al., 2012, Yamaguchi et al., 2009).

3.3. Kinematic calculations

Most articles that defined a coordinate system provided corresponding kinematic calculations, but two articles only described kinematic calculations (Wan et al., 2006, Xu et al., 2015) and six articles lacked kinematic calculations (Claassen et al., 2019, Green et al., 2011, Hayes et al., 2006). There are three primary ways authors in this review defined kinematic calculations: joint coordinate system (JCS), Cardan/Euler angle sequences, or helical angles.

3.3.1. Joint coordinate system (JCS)

The JCS as described by Grood and Suntay describes a method to calculate rotation and translation about three axes using two axes fixed to the distal and proximal segments and a third "floating axis" that is mutually perpendicular (Grood and Suntay, 1983). Fifteen articles used a JCS either as described by the ISB standard or used other axis definitions to describe kinematic calculations (Table 6). The most common method of JCS followed the convention described by the ISB standard for the ankle joint complex which defines the ML axis as the primary axis and AP axis as the secondary axis for both the tibiotalar and subtalar joints. This method was used by ten articles in this review to calculate tibiotalar and/or subtalar kinematics (Chen Wang et al., 2016, Fukano and Fukubayashi, 2014, Fukano et al., 2018, Fukano et al., 2020, Koo et al., 2015, Lenz et al., 2020, Roach et al., 2017, Roach et al., 2016b, Wang et al., 2015a, Yamaguchi et al., 2009). All articles except two (Fukano et al., 2020, Lenz et al., 2020) also reported translation. Leszko et al. used this same convention to describe rotation and translation of a mobile bearing total ankle prosthesis (Leszko et al., 2008).

Table 6. Kinematic calculations.

Kinematic Methods	**Rotation Sequence/Axes Definition**	**Reported Translations (Y/N)**	**Articles Using Method**
Joint Coordinate System	**Primary Axis**: Mediolateral**Secondary Axis**: Anteroposterior	Y	(Chen Wang et al., 2016)
		Y	(Fukano and Fukubayashi, 2014)
		Y	(Fukano et al., 2018)
		N	(Fukano et al., 2020)
		Y	(Koo et al., 2015)
		N	(Lenz et al., 2020)
		Y	(Leszko et al., 2008)
		Y	(Roach et al., 2016a, Roach et al., 2016a)
		Y	(Roach et al., 2017)
		Y	(Wang et al., 2015a, Wang et al., 2015b)
		Y	(Yamaguchi et al., 2009)
	Primary Axis: Mediolateral **Secondary Axis**: Superoinferior	Y	(Van Sint Jan et al., 2006)
		Y	(Caputo et al., 2009)
	Primary Axis: Anteroposterior**Secondary Axis**: Mediolateral	Y	(Wainright et al., 2012)

		Y	(Zhang et al., 2019)
Cardan Angles	Sagittal, Coronal, Transverse	Y	(de Asla et al., 2006)
		Y	(Ito et al., 2015)
		Y	(Kobayashi et al., 2013)
		Y	(Kobayashi et al., 2014a)
		Y	(Kobayashi et al., 2014b)
		Y	(Kobayashi et al., 2015)
		Y	(Kozanek et al., 2009)
		N	(Nichols et al., 2016)
		N	(Nichols et al., 2017)
		N	(Wan et al., 2006)
	Sagittal Transverse, Coronal	Y	(Imai et al., 2011)
		Y	(Imai et al., 2009)
		Y	(Makki et al., 2019)
		Y	(Mattingly et al., 2006)
	Coronal, Transverse, Sagittal	Y	(Iwamoto et al., 2014)
		Y	(Liu et al., 2007)
	Unspecified	Y	(Cao et al., 2019a)
		Y	(Cao et al., 2019b)
		N	(Ledoux et al., 2006)
		Y	(Maharaj et al., 2020)
Helical Axis	n/a	n/a	(Beimers et al., 2008, Cho et al., 2014, Clarke et al., 2015, Fassbind et al., 2011, Goto et al., 2009, Kleipool et al., 2019; Kleipool et al., 2016; Parr et al., 2012, Wolf et al., 2007, Wolf et al., 2008)

Two other axes definitions were identified. Two articles (Caputo et al., 2009, Van Sint Jan et al., 2006) defined a primary ML axis and a secondary SI axis as described by other literature (Cappozzo et al., 1995, Leardini et al., 1999). Two of the included articles defined a primary AP axis and a secondary ML axis (Wainright et al., 2012, Zhang et al., 2019).

3.3.2. Cardan/Euler

Cardan/Euler angles (Ayoub et al., 1974, Goldstein, 1980, Tupling and Pierrynowski, 1987) are used to describe the orientation of a rigid body with respect to a fixed coordinate system. These angles describe those with which a coordinate system must be rotated in a defined sequence about embedded orthogonal axes to map it from that of the proximal body segment coordinate system to that of the distal. In standard convention, Cardan angles require rotations about three axes (e.g. YXZ) while strict Euler angles require the third rotation to be a repeat of the first (e.g. ZXZ). However, in biomechanics literature, both Euler and Cardan terminology has been used by various authors to describe rotation sequences about three unique axes. Therefore, this review will refer to all sequences using Cardan/Euler angle terminology to describe these methods to emphasize their equivalence.

A total of 20 articles in this review used Cardan/Euler sequences to calculate kinematics. The most common sequence was sagittal/coronal/transverse and used by 10 included articles (de Asla et al., 2006, Ito et al., 2015, Kobayashi et al., 2013, Kobayashi et al., 2014a, Kobayashi et al., 2015, Kozanek et al., 2009, Nichols et al., 2016, Nichols et al., 2017, Wan et al., 2006). Other sequences used included sagittal/transverse/coronal which was used by four articles (Imai et al., 2011, Imai et al., 2009, Makki et al., 2019, Mattingly et al., 2006) and

coronal/transverse/sagittal which was used by two articles (Iwamoto et al., 2014, Liu et al., 2007). Four additional papers also reported using Cardan/Euler sequences but did not specify a rotation order (Cao et al., 2019a, Ledoux et al., 2006, Maharaj et al., 2020). Of the included articles, 16/20 that used Cardan/Euler sequences also reported translations with a majority using either previously undescribed or undocumented methods (Table 6). Two articles (Cao et al., 2019a,b) calculated joint translations by subtracting the origin location of one bone from the origin location of an adjacent bone (Zhu and Li, 2012).

3.3.3. Helical angles

Ten articles used helical angles to describe their kinematic calculations which often include a deviation and inclination angle. Previous definitions (Woltring et al., 1985, Woltring et al., 1994) were combined to describe a helical axis for subtalar motion (Beimers et al., 2008, Parr et al., 2012, Van Sint Jan et al., 2006). Based on a previously described definition (Parr et al., 2012) and a self-defined system, an article (Cho et al., 2014) defined the deviation angle of the talocrural joint axis as the angle between the second principal direction and talocrural joint axis on the transverse plane and the inclination angle as the angle between the third principal direction and talocrural joint axis on the coronal plane. The paper described a different definition for the subtalar joint axis where the deviation angle was defined as the angle between the principal axis and subtalar joint axis on the transverse plane and the inclination angle was defined as the angle between first principal direction and the subtalar joint axis on the sagittal plane. Two articles (Clarke et al., 2015, Goto et al., 2009) use rigid-body transformations to calculate the pose of the helical axis via the helical screw axis technique (Spoor and Veldpaus, 1980). One article (Fassbind et al., 2011) used several established finite helical axis calculations (Schmidt, 1985) to determine kinematics. Two ICP-based articles (Wolf et al., 2007, Wolf et al., 2008) used a series of finite helical axis rotations projected onto cardinal body planes to describe kinematic calculations (Besl and McKay, 1992). Kleipool et al. used a cylinder fit to the posterior facet of the calcaneus to describe the inclination and deviation angles. The inclination angle was between the cylinder's axis and the transverse plane while the deviation angle was between the cylinder's axis and the AP axis.

4. Discussion

The goal of this systematic review was to provide a summary of existing literature that defined coordinate systems for the tibia, talus, and/or calcaneus and assigned kinematic mathematical definitions for the tibiotalar or subtalar joints. Previous literature used geometric or landmark-based ACSs, principal axes, ICP registration, of a combination of these methods to assign local coordinate systems to these bones. The JCS, Cardan/Euler sequences, and helical axes were used to compute tibiotalar and subtalar kinematics.

4.1. Evaluation of local coordinate systems

Articles in this review used a combination of automated, semi-automated, and manual identification methods to assign local coordinate systems to individual bones. Automated methods such as principal axes are advantageous because they do not require user definitions however, they may not represent the true joint axes. A previous morphology study showed that in the case of the calcaneus, the second and third principal axes do not accurately represent clinical terminology used to characterize frontal plane anatomy (Brown et al., 2020). Studies using manual or semi-automated methods to identify individual landmarks or geometric feature are susceptible to inter and intra-user variability, with one study reporting variability in deviation angles computed from manually defined points ranging from 2.8° to 7.4° (Brown et al., 2020). Therefore, it is important for studies using these methods to document reliability metrics when establishing new coordinate system definitions. Coordinate system definitions can be highly variable based shapes of the individual bones which can vary based on foot type, age, or symptomatic pathology (e.g. cerebral palsy, Charcot-Marie-Tooth disease, or osteoarthritis) (Miller, 2019, Nelson et al., 2017, Schaefer et al., 2012, Schwend and Drennan, 2003). One paper in this review analyzed both pes cavus and pes planus foot types (Ledoux et al., 2006). All other included papers focused on

either asymptomatic individuals or comparison to a single pathologic group. For a method of assigning local coordinate systems to gain universal acceptance, it must consider these anatomic variations of foot shape and patient populations. Future work is needed to evaluate these existing coordinate systems to evaluate which definitions can be reliability applied to multiple foot pathologies (e.g. cerebral palsy, Charcot-Marie-Tooth disease, or osteoarthritis) while capturing their anatomic variability.

In this review, several articles defined coordinate systems of individual bones based on their individual anatomy while others defined the axes of the talus and calcaneus as parallel to the tibia axes during standing. A previous comparison of these two methods reported shifts in kinematic curves of up to 45° and range of motion differences of up to 6° in all three planes of motion (Kruger et al., 2019b). This finding is consistent with a previous parametric study by Long et at. showed that when the hindfoot orientation angles were perturbed as little as 2° from their true orientation, significant shifts to the kinematic curves resulted (Long et al., 2008). This further confirms the importance of accurately representing skeletal alignment given that the variability in measures of foot structure far exceed 2° even within the healthy, asymptomatic population (Hillstrom et al., 2013).

4.2. Kinematics

When Cardan/Euler sequences are used to calculate kinematics, conventional biomechanics convention is to order rotations in a sagittal/coronal/transverse sequence for lower extremity kinematics (Kadaba et al., 1990). Consistent with this convention, sagittal/coronal/transverse was the most common rotation sequence used in studies included in this review. While this sequence may be appropriate for the tibiotalar joint, previous biplane fluoroscopy work has shown higher subtalar joint range of motion in the coronal and transverse planes (de Asla et al., 2006, Roach et al., 2016a), indicating this rotation sequence may not be the most appropriate to use. Additionally, pathology is likely to cause range of motion differences, therefore it is important to be able to capture extreme ranges of motion most likely to be encountered within different pathologies.

The ISB standards are citied by papers included in this review using the JCS. It has been commonly espoused that the JCS axis arrangement creates a unique set of angles which are independent of the order in which they are described. The JCS methodology does however require that a fixed axis must be assigned to each rigid body. Mathematical proofs have shown the JCS and Cardan sequences are equivalent, thus they are sequence dependent and orthogonal (Baker, 2003, MacWilliams and Davis, 2013). The JCS description does however, include a specific description of joint translations. Several papers in this review that used Cardan angles to report kinematics also reported joint translation, however, they scored lower on our assessment of methodologic quality due to using either undescribed or unvalidated methods to compute translation.

Finite or instantaneous helical axes are a potentially effective tool for joint kinematic analysis. At each moment in time, the motion of a rigid body can be broken down into a rotation about, and a translation along, a single axis. A limitation of the helical axis method, however, is that when the helical rotation is zero, the helical axis is undefined. This makes this approach susceptible to error with small rotations based on the data quality (McLachlin et al., 2014, Woltring et al., 1985). This limitation potentially makes this approach less desirable for joints such as at subtalar joint where rotations in multiple planes are small.

Reliable and consistent methods of neutral referencing are crucial for repeatable kinematic results. This topic has been remarked upon in literature regarding segmental foot models. Previous work has shown conflicting segmental kinematic results with similar subject populations, likely due to differences in neutral referencing (Buldt et al., 2015, Kruger et al., 2019a). Neutral referencing is achieved through methods including comfortable standing, subtalar neutral, and radiographic indexing. Use of a “zero reference level” from comfortable standing or subtalar neutral is limited because it removes joint alignment differences which are frequently used as part of clinical assessment and should be included in the analysis (Leardini and Caravaggi, 2017). This also has the

potential to negate differences in bone geometric shape and/or alignment in pathologies such as osteoarthritis (Wang et al., 2015b) and cerebral palsy (Kruger et al., 2017) and even within asymptomatic, healthy populations (Krähenbühl et al., 2020).

4.3. Quality assessment

The critical evaluation of each article resulted in a methodologic score that was a useful mode of describing each article and comparing articles by those metrics. The highest scoring articles at 97 (Fukano et al., 2018, Fukano et al., 2020, Lenz et al., 2020, Roach et al., 2016b) provided in-depth descriptions that detailed the extent of their research and provided sufficient information for reproducibility. The lowest methodologic score was 61 (Parr et al., 2012) which lacked adequate descriptions in two of the most commonly under described categories – clinical implications of results and consistency of findings. On average, the lowest scoring categories were a discussion of the clinical implications of the results, consistency of findings, and a description of kinematic modeling. Low scores in consistency of findings indicated authors did not adequately perform data reliability or validation checks. This is especially important given the new imaging modalities used (e.g. WBCT) and the uniqueness of how each experimental fluoroscopy setup was used. Articles with low description of kinematic modeling scores had poorly described coordinate system and/or modeling definitions. It is important that all aspects of kinematic modeling are adequately reported to allow for reproducibility of methods in future studies. Articles in this review utilized helical axes, JCS, and Cardan/Euler angles to model the ankle joint complex. The lack of consistency in describing these methods, as can be noted by the low methodologic average score, reaffirms the need for a universal and well described coordinate system with kinematic modeling method.

Of the included articles that incorporated dynamic fluoroscopy tracking of bones, 11 used a single fluoroscopy system while 17 used a biplane system (Table 3). While using a system with a single fluoroscopy unit to measure joint motion has advantages including decreased radiation and equipment cost, caution should be taken when interpreting single plane results because it has poor out-of-plane accuracy (Fregly et al., 2005, Kapron et al., 2014). For single-plane use, the fluoroscope must be positioned carefully to obtain sufficient bony details from optimized viewing angles, while minimizing occlusion of surrounding tissues and out-of-plane movement for the analyzed activity (Lin et al., 2013). Therefore, results of single plane fluoroscopy should be interpreted with a degree of caution, especially with out-of-plane rotations. Additionally, when any kinematics are reported from a dynamic fluoroscopy system, it is important that each laboratory's system be validated for each joint being analyzed.

5. Conclusions

Following almost two decades since the ISB standard was published, researchers have creatively defined numerous methods for establishing tibia, talus and/or calcaneus coordinate systems and related kinematic rotations due to the lack of a unified standard. With the emergence of biplane fluoroscopy to capture *in vivo* kinematics, the necessity to accurately define tibiotalar and subtalar motion has become evident. The presentation of 52 articles containing various methodological definitions for coordinate systems and kinematics was conducted with the intention of providing a succinct resource for the foot and ankle community. Ultimately this review article may lead to collaborative discussions to develop a useful standard that will facilitate improved clinical evaluation of *in vivo* hindfoot kinematics.

Acknowledgements

Funding provided by Shriners Hospitals for Children (#79146).

References

Ayoub et al., 1974 M.A. Ayoub, M.M. Ayoub, A.G. Walvekar. **A biomechanical model for the upper extremity using optimization techniques.** Hum. Factors, 16 (1974), pp. 585-594

Baker, 2003 R. Baker. **ISB recommendation on definition of joint coordinate systems for the reporting of human joint motion-part I: ankle, hip and spine.** J. Biomech., 36 (2003), pp. 300-302. author reply 303–304

Barg et al., 2018 A. Barg, T. Bailey, M. Richter, C. de Cesar Netto, F. Lintz, A. Burssens, P. Phisitkul, C.J. Hanrahan, C.L. Saltzman. **Weightbearing computed tomography of the foot and ankle: emerging technology topical review.** Foot Ankle Int., 39 (2018), pp. 376-386

Beimers et al., 2008 L. Beimers, G.J. Tuijthof, L. Blankevoort, R. Jonges, M. Maas, C.N. van Dijk. **In-vivo range of motion of the subtalar joint using computed tomography.** J. Biomech., 41 (2008), pp. 1390-1397

Besl and McKay, 1992 P.J. Besl, H.D. McKay. **A method for registration of 3-D shapes.** IEEE Trans. Pattern Anal. Mach. Intell., 14 (1992), pp. 239-256

Brown et al., 2020 J.A. Brown, T. Gale, W. Anderst. **An automated method for defining anatomic coordinate systems in the hindfoot.** J. Biomech., 109 (2020), p. 109951

Buldt et al., 2015 A.K. Buldt, P. Levinger, G.S. Murley, H.B. Menz, C.J. Nester, K.B. Landorf. **Foot posture is associated with kinematics of the foot during gait: a comparison of normal, planus and cavus feet.** Gait Posture, 42 (2015), pp. 42-48

Campbell et al., 2016 K.J. Campbell, K.J. Wilson, R.F. LaPrade, T.O. Clanton. **Normative rearfoot motion during barefoot and shod walking using biplane fluoroscopy.** Knee Surg. Sports Traumatol. Arthros.: Off. J. ESSKA, 24 (2016), pp. 1402-1408

Cao et al., 2019a S. Cao, C. Wang, G. Zhang, X. Ma, X. Wang, J. Huang, C. Zhang, K. Wang. **Effects of an ankle brace on the in vivo kinematics of patients with chronic ankle instability during walking on an inversion platform.** Gait Posture, 72 (2019), pp. 228-233

Cao et al., 2019b S. Cao, C. Wang, G. Zhang, X. Ma, X. Wang, J. Huang, C. Zhang, K. Wang. **In vivo kinematics of functional ankle instability patients during the stance phase of walking.** Gait Posture, 73 (2019), pp. 262-268

Cappozzo et al., 1995 A. Cappozzo, F. Catani, U.D. Croce, A. Leardini. **Position and orientation in space of bones during movement: anatomical frame definition and determination.** Clin. Biomech. (Bristol, Avon), 10 (1995), pp. 171-178

Caputo et al., 2009 A.M. Caputo, J.Y. Lee, C.E. Spritzer, M.E. Easley, J.K. DeOrio, J.A. Nunley 2nd, L.E. DeFrate. **In vivo kinematics of the tibiotalar joint after lateral ankle instability.** Am. J. Sports Med., 37 (2009), pp. 2241-2248

Chen Wang et al., 2016 M.D. Chen Wang, X. Geng, S. Wang, M.D. Xin Ma, M.D. Xu Wang, M.D. Jiazhang Huang, M.D. Chao Zhang, M.S. Li Chen, J. Yang, K. Wang. **In vivo kinematic study of the tarsal joints complex based on fluoroscopic 3D–2D registration technique.** Gait Posture, 49 (2016), pp. 54-60

Cho et al., 2014 H.J. Cho, D.S. Kwak, I.B. Kim. **Analysis of movement axes of the ankle and subtalar joints: relationship with the articular surfaces of the talus.** Proc. Inst. Mech. Eng. H, 228 (2014), pp. 1053-1058

Claassen et al., 2019 L. Claassen, P. Luedtke, D. Yao, S. Ettinger, K. Daniilidis, A.M. Nowakowski, M. Mueller-Gerbl, C. Stukenborg-Colsman, C. Plaass. **The geometrical axis of the talocrural joint-suggestions for a new measurement of the talocrural joint axis.** Foot Ankle Surg., 25 (2019), pp. 371-377

Clarke et al., 2015 E.C. Clarke, J.H. Martin, A.G. d'Entremont, M.G. Pandy, D.R. Wilson, R.D. Herbert. **A non-invasive, 3D, dynamic MRI method for measuring muscle moment arms in vivo: demonstration in the human ankle joint and Achilles tendon.** Med. Eng. Phys., 37 (2015), pp. 93-99

Cross et al., 2017 J.A. Cross, B.D. McHenry, R. Molthen, E. Exten, T.G. Schmidt, G.F. Harris. **Biplane fluoroscopy for hindfoot motion analysis during gait: a model-based evaluation.** Med. Eng. Phys., 43 (2017), pp. 118-123

de Asla et al., 2006 R.J. de Asla, L. Wan, H.E. Rubash, G. Li. **Six DOF in vivo kinematics of the ankle joint complex: application of a combined dual-orthogonal fluoroscopic and magnetic resonance imaging technique.** J. Orthop. Res., 24 (2006), pp. 1019-1027

Fassbind et al., 2011 M.J. Fassbind, E.S. Rohr, H. Yangqiu, D.R. Haynor, S. Siegler, B.J. Sangeorzan, W.R. Ledoux. **Evaluating foot kinematics using magnetic resonance imaging: from maximum plantar flexion, inversion, and internal rotation to maximum dorsiflexion, eversion, and external rotation.** J. Biomech. Eng., 133 (2011), pp. 104502-104507

Fregly et al., 2005 B.J. Fregly, H.A. Rahman, S.A. Banks. **Theoretical accuracy of model-based shape matching for measuring natural knee kinematics with single-plane fluoroscopy.** J. Biomech. Eng., 127 (2005), pp. 692-699

Fukano and Fukubayashi, 2014 M. Fukano, T. Fukubayashi. **Changes in talocrural and subtalar joint kinematics of barefoot versus shod forefoot landing.** J Foot Ankle Res, 7 (2014), p. 42

Fukano et al., 2018 M. Fukano, T. Fukubayashi, S.A. Banks. **Sex differences in three-dimensional talocrural and subtalar joint kinematics during stance phase in healthy young adults.** Hum. Mov. Sci., 61 (2018), pp. 117-125

Fukano et al., 2020 M. Fukano, T. Fukubayashi, T. Kumai. **In vivo talocrural and subtalar kinematics during the stance phase of walking in individuals with repetitive ankle sprains.** J. Biomech., 101 (2020), p. 109651

Goldstein, 1980 Goldstein, H., 1980. Classical Mechanics, 2nd ed. Addison-Wesle, ading, MA.

Goto et al., 2009 A. Goto, H. Moritomo, T. Itohara, T. Watanabe, K. Sugamoto. **Three-dimensional in vivo kinematics of the subtalar joint during dorsi-plantarflexion and inversion-eversion.** Foot Ankle Int., 30 (2009), pp. 432-438

Green et al., 2011 C. Green, C. Fitzpatrick, D. FitzPatrick, M. Stephens, W. Quinlan, R. Flavin. **Definition of coordinate system for three-dimensional data analysis in the foot and ankle.** Foot Ankle Int., 32 (2011), pp. 193-199

Grood and Suntay, 1983 E.S. Grood, W.J. Suntay. **A joint coordinate system for the clinical description of three-dimensional motions: application to the knee.** J. Biomech. Eng., 105 (1983), pp. 136-144

Gutekunst et al., 2013 D.J. Gutekunst, L. Liu, T. Ju, F.W. Prior, D.R. Sinacore. **Reliability of clinically relevant 3D foot bone angles from quantitative computed tomography.** J. Foot Ankle Res., 6 (2013), p. 38

Hayes et al., 2006 A. Hayes, Y. Tochigi, C.L. Saltzman. **Ankle morphometry on 3D-CT images.** Iowa Orthop. J., 26 (2006), pp. 1-4

Hillstrom et al., 2013
H.J. Hillstrom, J. Song, A.P. Kraszewski, J.F. Hafer, R. Mootanah, A.B. Dufour, B.S. Chow, J.T. Deland 3rd. **Foot type biomechanics part 1: structure and function of the asymptomatic foot.** Gait Posture, 37 (2013), pp. 445-451

Imai et al., 2011 K. Imai, K. Ikoma, M. Maki, M. Kido, Y. Tsuji, R. Takatori, D. Tokunaga, N. Inoue, T. Kubo. **Features of hindfoot 3D kinetics in flat foot in ankle-joint maximal dorsiflexion and plantarflexion.** J. Orthop. Sci., 16 (2011), pp. 638-643

Imai et al., 2009
K. Imai, D. Tokunaga, R. Takatori, K. Ikoma, M. Maki, H. Ohkawa, A. Ogura, Y. Tsuji, N. Inoue, T. Kubo. **In vivo three-dimensional analysis of hindfoot kinematics.** Foot Ankle Int., 30 (2009), pp. 1094-1100

Ito et al., 2015
K. Ito, K. Hosoda, M. Shimizu, S. Ikemoto, S. Kume, T. Nagura, N. Imanishi, S. Aiso, M. Jinzaki, N. Ogihara. **Direct assessment of 3D foot bone kinematics using biplanar X-ray fluoroscopy and an automatic model registration method.** J. Foot Ankle Res., 8 (2015), p. 21

Iwamoto et al., 2014 K. Iwamoto, K. Shi, T. Tomita, J. Hashimoto, T. Yamazaki, H. Yoshikawa, K. Sugamoto. **In vivo kinematics of three-component mobile-bearing total ankle replacement in rheumatoid ankle with talocalcaneal arthrodesis and spontaneous talocalcaneal fusion.** Mod. Rheumatol., 24 (2014), pp. 897-903

Kadaba et al., 1990 M.P. Kadaba, H.K. Ramakrishnan, M.E. Wootten. **Measurement of lower extremity kinematics during level walking.** J. Orthop. Res., 8 (1990), pp. 383-392

Kapron et al., 2014 A.L. Kapron, S.K. Aoki, C.L. Peters, S.A. Maas, M.J. Bey, R. Zauel, A.E. Anderson. **Accuracy and feasibility of dual fluoroscopy and model-based tracking to quantify in vivo hip kinematics during clinical exams.** J. Appl. Biomech., 30 (2014), pp. 461-470

Kleipool et al., 2016 R.P. Kleipool, J.J. Natenstedt, G.J. Streekstra, J.G. Dobbe, R.M. Gerards, L. Blankevoort, G.J. Tuijthof. **The Mechanical Functionality of the EXO-L Ankle Brace: Assessment With a 3-Dimensional Computed Tomography Stress Test.** Am J Sports Med, 44 (2016), pp. 171-176

Kleipool et al., 2019 R.P. Kleipool, J. Dahmen, G. Vuurberg, R.J. Oostra, L. Blankevoort, M. Knupp, S.A.S. Stufkens. **Study on the three-dimensional orientation of the posterior facet of the subtalar joint using simulated weight-bearing CT.** J. Orthop. Res., 37 (2019), pp. 197-204

Kobayashi et al., 2013 T. Kobayashi, Y. No, K. Yoneta, M. Sadakiyo, K. Gamada. **In vivo kinematics of the talocrural and subtalar joints with functional ankle instability during weight-bearing ankle internal rotation: a pilot study.** Foot Ankle Spec., 6 (2013), pp. 178-184

Kobayashi et al., 2014a T. Kobayashi, M. Saka, E. Suzuki, N. Yamazaki, M. Suzukawa, A. Akaike, K. Shimizu, K. Gamada. **The effects of a semi-rigid brace or taping on talocrural and subtalar kinematics in chronic ankle instability.** Foot Ankle Spec., 7 (2014), pp. 471-477

Kobayashi et al., 2014b T. Kobayashi, M. Saka, E. Suzuki, N. Yamazaki, M. Suzukawa, A. Akaike, K. Shimizu, K. Gamada. **In vivo kinematics of the talocrural and subtalar joints during weightbearing ankle rotation in chronic ankle instability.** Foot Ankle Spec., 7 (2014), pp. 13-19

Kobayashi et al., 2015 T. Kobayashi, E. Suzuki, N. Yamazaki, M. Suzukawa, A. Akaike, K. Shimizu, K. Gamada. **In vivo talocrural joint contact mechanics with functional ankle instability.** Foot Ankle Spec., 8 (2015), pp. 445-453

Koo et al., 2015 S. Koo, K.M. Lee, Y.J. Cha. **Plantar-flexion of the ankle joint complex in terminal stance is initiated by subtalar plantar-flexion: a bi-planar fluoroscopy study.** Gait Posture, 42 (2015), pp. 424-429

Kozanek et al., 2009 M. Kozanek, H.E. Rubash, G. Li, R.J. de Asla. **Effect of post-traumatic tibiotalar osteoarthritis on kinematics of the ankle joint complex.** Foot Ankle Int., 30 (2009), pp. 734-740

Krähenbühl et al., 2020 N. Krähenbühl, A.L. Lenz, R.J. Lisonbee, A.C. Peterson, P.R. Atkins, B. Hintermann, C.L. Saltzman, A.E. And erson, A. Barg. **Morphologic analysis of the subtalar joint using statistical shape modeling.** J. Orthop. Res., 38 (2020), pp. 2625-2633

Kruger et al., 2019a K.M. Kruger, A. Graf, A. Flanagan, B.D. McHenry, H. Altiok, P.A. Smith, G.F. Harris, J.J. Krzak. **Segmental foot and ankle kinematic differences between rectus, planus, and cavus foot types.** J. Biomech., 94 (2019), pp. 180-186

Kruger et al., 2019b K.M. Kruger, J. Krzak, B.D. McHenry, A. Flanagan, A. Graf, H. Altiok, P.A. Smith, G.F. Harris. **Comparative analysis of anatomic coordinate systems to calculate hindfoot kinematics using biplane fluoroscopy.** Biomed. Sci. lnstrum., 55 (2019), pp. 373-378

Kruger et al., 2017 K.M. Kruger, K.A. Konop, J.J. Krzak, A. Graf, H. Altiok, P.A. Smith, G.F. Harris. **Segmental kinematic analysis of planovalgus feet during walking in children with cerebral palsy.** Gait Posture, 54 (2017), pp. 277-283

Leardini and Caravaggi, 2017 A. Leardini, P. Caravaggi. **Kinematic foot models for instrumented gait analysis.** B. Müller, S.I. Wolf, G.-.P. Brueggemann, Z. Deng, A. McIntosh, F. Miller, W.S. Selbie (Eds.), Handbook of Human Motion, Springer International Publishing, Cham (2017), pp. 1-24

Leardini et al., 1999 A. Leardini, J.J. O'Connor, F. Catani, S. Giannini. **Kinematics of the human ankle complex in passive flexion; a single degree of freedom system.** J. Biomech., 32 (1999), pp. 111-118

Ledoux et al., 2006 W.R. Ledoux, E.S. Rohr, R.P. Ching, B.J. Sangeorzan. **Effect of foot shape on the three-dimensional position of foot bones.** J. Orthop. Res., 24 (2006), pp. 2176-2186

Lenz et al., 2020 A.L. Lenz, J.A. Nichols, K.E. Roach, K.B. Foreman, A. Barg, C.L. Saltzman, A.E. Anderson. **Compensatory motion of the subtalar joint following tibiotalar arthrodesis: an in vivo dual-fluoroscopy imaging study.** J. Bone Joint Surg. Am., 102 (2020), pp. 600-608

Leszko et al., 2008 F. Leszko, R.D. Komistek, M.R. Mahfouz, Y.A. Ratron, T. Judet, M. Bonnin, J.A. Colombier, S.S. Lin. **In vivo kinematics of the salto total ankle prosthesis.** Foot Ankle Int., 29 (2008), pp. 1117-1125

Lin et al., 2013 H. Lin, S. Wang, T.-Y. Tsai, G. Li, Y.-M. Kwon. **In-vitro validation of a non-invasive dual fluoroscopic imaging technique for measurement of the hip kinematics.** Med. Eng. Phys., 35 (2013), pp. 411-416

Liu et al., 2007 H. Liu, K. Sugamoto, T. Itohara, T. Tomita, J. Hashimoto, H. Yoshikawa. **In vivo three-dimensional skeletal alignment analysis of the hindfoot valgus deformity in patients with rheumatoid arthritis.** J. Orthop. Res., 25 (2007), pp. 330-339

Long et al., 2008 J.T. Long, M. Wang, J.M. Winters, G.F. Harris. **A multisegmental foot model with bone-based referencing: sensitivity to radiographic input parameters.** Conf Proc IEEE Eng Med Biol Soc, 2008 (2008), pp. 879-882

MacWilliams et al., 2003 B.A. MacWilliams, M. Cowley, D.E. Nicholson. **Foot kinematics and kinetics during adolescent gait.** Gait Posture, 17 (2003), pp. 214-224

MacWilliams and Davis, 2013 B.A. MacWilliams, R.B. Davis. **Addressing some misperceptions of the joint coordinate system.** J. Biomech. Eng., 135 (2013), p. 54506

Maharaj et al., 2020 J.N. Maharaj, S. Kessler, M.J. Rainbow, S.E. D'Andrea, N. Konow, L.A. Kelly, G.A. Lichtwark. **The reliability of foot and ankle bone and joint kinematics measured with biplanar videoradiography and manual scientific rotoscoping.** Front. Bioeng. Biotechnol., 8 (2020), p. 106

Makki et al., 2019 K. Makki, B. Borotikar, M. Garetier, S. Brochard, D. Ben Salem, F. Rousseau. **In vivo ankle joint kinematics from dynamic magnetic resonance imaging using a registration-based framework.** J. Biomech., 86 (2019), pp. 193-203

Maslen and Ackland, 1994 B.A. Maslen, T.R. Ackland. **Radiographic study of skin displacement errors in the foot and ankle during standing.** Clin. Biomech. (Bristol, Avon), 9 (1994), pp. 291-296

Mattingly et al., 2006 B. Mattingly, V. Talwalkar, C. Tylkowski, D.B. Stevens, P.A. Hardy, D. Pienkowski. **Three-dimensional in vivo motion of adult hind foot bones.** J. Biomech., 39 (2006), pp. 726-733

McLachlin et al., 2014 S.D. McLachlin, L.M. Ferreira, C.E. Dunning. **A refined technique to calculate finite helical axes from rigid body trackers.** J. Biomech. Eng., 136 (2014), p. 124506

Miller, 2019 F. Miller. **Planovalgus foot deformity in cerebral palsy.** F. Miller, S. Bachrach, N. Lennon, M. O'Neil (Eds.), Cerebral Palsy, Springer International Publishing, Cham (2019), pp. 1-40

Nelson et al., 2017 A.E. Nelson, Y.M. Golightly, S. Lateef, J.B. Renner, J.M. Jordan, R.M. Aspden, H. Hillstrom, J.S. Gregory. **Cross-sectional associations between variations in ankle shape by statistical shape modeling, injury history, and race: the Johnston County Osteoarthritis Project.** J. Foot Ankle Res., 10 (2017), p. 34

Nichols et al., 2016 J.A. Nichols, K.E. Roach, N.M. Fiorentino, A.E. Anderson. **Predicting tibiotalar and subtalar joint angles from skin-marker data with dual-fluoroscopy as a reference standard.** Gait Posture, 49 (2016), pp. 136-143

Nichols et al., 2017 J.A. Nichols, K.E. Roach, N.M. Fiorentino, A.E. Anderson. **Subject-specific axes of rotation based on talar morphology do not improve predictions of tibiotalar and subtalar joint kinematics.** Ann. Biomed. Eng., 45 (2017), pp. 2109-2121

Nozaki et al., 2016 S. Nozaki, K. Watanabe, M. Katayose. **Three-dimensional analysis of talar trochlea morphology: implications for subject-specific kinematics of the talocrural joint.** Clin. Anat., 29 (2016), pp. 1066-1074

Nozaki et al., 2017 S. Nozaki, K. Watanabe, M. Katayose. **Three-dimensional morphometric analysis of the talus: implication for variations in kinematics of the subtalar joint. Surg Radiol Anat 39, 1097–1106. Okita,**

N., Meyers, S.A., Challis, J.H., Sharkey, N.A., 2014. Midtarsal joint locking: New perspectives on an old paradigm. Journal of Orthopaedic Research, 32 (2017), pp. 110-115

Nozaki et al., 2019 S. Nozaki, K. Watanabe, T. Kato, T. Miyakawa, T. Kamiya, M. Katayose. **Radius of curvature at the talocrural joint surface: inference of subject-specific kinematics.** Surg. Radiol. Anat., 41 (2019), pp. 53-64

Ochia et al., 2006 R.S. Ochia, N. Inoue, S.M. Renner, E.P. Lorenz, T.H. Lim, G.B. Andersson, H.S. An. **Three-dimensional in vivo measurement of lumbar spine segmental motion.** Spine (Phila Pa 1976), 31 (2006), pp. 2073-2078

Parr et al., 2012 W.C. Parr, H.J. Chatterjee, C. Soligo. **Calculating the axes of rotation for the subtalar and talocrural joints using 3D bone reconstructions.** J. Biomech., 45 (2012), pp. 1103-1107

Roach et al., 2017 K.E. Roach, K.B. Foreman, A. Barg, C.L. Saltzman, A.E. Anderson. **Application of high-speed dual fluoroscopy to study in vivo tibiotalar and subtalar kinematics in patients with chronic ankle instability and asymptomatic control subjects during dynamic activities.** Foot Ankle Int., 38 (2017), pp. 1236-1248

Roach et al., 2016a K.E. Roach, B. Wang, A.L. Kapron, N.M. Fiorentino, C.L. Saltzman, K. Bo Foreman, A.E. Anderson. **In vivo kinematics of the tibiotalar and subtalar joints in asymptomatic subjects: a high-speed dual fluoroscopy study.** J. Biomech. Eng., 138 (2016)

Roach et al., 2016b K.E. Roach, B. Wang, A.L. Kapron, N.M. Fiorentino, C.L. Saltzman, K.B. Foreman. **In vivo kinematics of the tibiotalar and subtalar joints in asymptomatic subjects: a high-speed dual fluoroscopy study.** J. Biomech. Eng., 138 (2016)

Schaefer et al., 2012 K.L. Schaefer, B.J. Sangeorzan, M.J. Fassbind, W.R. Ledoux. **The comparative morphology of idiopathic ankle osteoarthritis.** JBJS, 94 (2012), p. e181

Schmidt, 1985 H.-J. Schmidt. **J. S. Beggs: kinematics. Hemisphere P. C. Washington und Springer Verlag Berlin 1983. XVI + 223 Seitcn, 64,- DM.** Astron. Nachr., 306 (1985), p. 62

Schwend and Drennan, 2003 R.M. Schwend, J.C. Drennan. **Cavus foot deformity in children.** JAAOS – J. Am. Acad. Orthopaedic Surg., 11 (2003), pp. 201-211

Spoor and Veldpaus, 1980 C.W. Spoor, F.E. Veldpaus. **Rigid body motion calculated from spatial co-ordinates of markers.** J. Biomech., 13 (1980), pp. 391-393

Trinler et al., 2018 U. Trinler, K. Hollands, R. Jones, R. Baker. **A systematic review of approaches to modelling lower limb muscle forces during gait: applicability to clinical gait analyses.** Gait Posture, 61 (2018), pp. 353-361

Tupling and Pierrynowski, 1987 S.J. Tupling, M.R. Pierrynowski. **Use of cardan angles to locate rigid bodies in three-dimensional space.** Med. Biol. Eng. Compu., 25 (1987), pp. 527-532

Van Sint Jan et al., 2006 S. Van Sint Jan, P. Salvia, V. Feipel, S. Sobzack, M. Rooze, V. Sholukha. **In vivo registration of both electrogoniometry and medical imaging: development and application on the ankle joint complex.** IEEE Trans. Biomed. Eng., 53 (2006), pp. 759-762

Wainright et al., 2012 W.B. Wainright, C.E. Spritzer, J.Y. Lee, M.E. Easley, J.K. DeOrio, J.A. Nunley, L.E. DeFrate. **The effect of modified Broström-Gould repair for lateral ankle instability on in vivo tibiotalar kinematics.** Am. J. Sports Med., 40 (2012), pp. 2099-2104

Wan et al., 2006 L. Wan, R.J. de Asla, H.E. Rubash, G. Li. **Determination of in-vivo articular cartilage contact areas of human talocrural joint under weightbearing conditions.** Osteoarthritis Cartilage, 14 (2006), pp. 1294-1301

Wang et al., 2015a B. Wang, K.E. Roach, A.L. Kapron, N.M. Fiorentino, C.L. Saltzman, M. Singer, A.E. Anderson. **Accuracy and feasibility of high-speed dual fluoroscopy and model-based tracking to measure in vivo ankle arthrokinematics.** Gait Posture, 41 (2015), pp. 888-893

Wang et al., 2015b B. Wang, C.L. Saltzman, O. Chalayon, A. Barg. **Does the subtalar joint compensate for ankle malalignment in end-stage ankle arthritis?** Clin. Orthop. Relat. Res., 473 (2015), pp. 318-325

Wilke et al., 2015 J. Wilke, F. Krause, D. Niederer, T. Engeroff, F. Nurnberger, L. Vogt, W. Banzer. **Appraising the methodological quality of cadaveric studies: validation of the QUACS scale.** J. Anat., 226 (2015), pp. 440-446

Wolf et al., 2007 P. Wolf, R. Luechinger, P. Boesiger, E. Stuessi, A. Stacoff. **A MR imaging procedure to measure tarsal bone rotations.** J. Biomech. Eng., 129 (2007), pp. 931-936

Wolf et al., 2008 P. Wolf, A. Stacoff, R. Luechinger, P. Boesiger, E. Stuessi. **Transmissions within the tarsal gearbox.** J. Am. Podiatr. Med. Assoc., 98 (2008), pp. 45-50

Woltring et al., 1985 H.J. Woltring, R. Huiskes, A. de Lange, F.E. Veldpaus. **Finite centroid and helical axis estimation from noisy landmark measurements in the study of human joint kinematics.** J. Biomech., 18 (1985), pp. 379-389

Woltring et al., 1994 H.J. Woltring, K. Long, P.J. Osterbauer, A.W. Fuhr. **Instantaneous helical axis estimation from 3-D video data in neck kinematics for whiplash diagnostics.** J. Biomech., 27 (1994), pp. 1415-1432

Wu et al., 2002 G. Wu, S. Siegler, P. Allard, C. Kirtley, A. Leardini, D. Rosenbaum, M. Whittle, D.D. D'Lima, L. Cristofolini, H. Witte, O. Schmid, I. Stokes, Standardization, Terminology Committee of the International Society of, B. **ISB recommendation on definitions of joint coordinate system of various joints for the reporting of human joint motion–part I: ankle, hip, and spine. International Society of Biomechanics.** J. Biomech., 35 (2002), pp. 543-548

Xu et al., 2015 J. Xu, Y. Zhang, H. Muhammad, X. Wang, J. Huang, C. Zhang, X. Geng, X. Ma. **In vivo three-dimensional analysis of hindfoot kinematics in stage II PTTD flatfoot.** J. Orthop. Sci., 20 (2015), pp. 488-497

Yamaguchi et al., 2009 S. Yamaguchi, T. Sasho, H. Kato, Y. Kuroyanagi, S.A. Banks. **Ankle and subtalar kinematics during dorsiflexion-plantarflexion activities.** Foot Ankle Int., 30 (2009), pp. 361-366

Yeung et al., 2015 T.W. Yeung, C.Y. Chan, W.C. Chan, Y.N. Yeung, M.K. Yuen. **Can pre-operative axial CT imaging predict syndesmosis instability in patients sustaining ankle fractures? Seven years' experience in a tertiary trauma center.** Skeletal Radiol., 44 (2015), pp. 823-829

Zhang et al., 2019 G. Zhang, S. Cao, C. Wang, X. Ma, X. Wang, J. Huang, C. Zhang. **Effect of a semirigid ankle brace on the in vivo kinematics of patients with functional ankle instability during the stance phase of walking.** Biomed. Res. Int., 2019 (2019), p. 4398469

Zhu and Li, 2012 Z. Zhu, G. Li. **An automatic 2D–3D image matching method for reproducing spatial knee joint positions using single or dual fluoroscopic images.** Comput. Methods Biomech. Biomed. Eng., 15 (2012), pp. 1245-1256